

Near-Infrared Chemiluminescent Carbon Nanodots and Their Application in Reactive Oxygen Species Bioimaging

Cheng-Long Shen, Qing Lou,* Jin-Hao Zang, Kai-Kai Liu, Song-Nan Qu, Lin Dong, and Chong-Xin Shan*

Reactive oxygen species (ROS) are generated in the body and related to many pathophysiological processes. Hence, detection of ROS is indispensable in understanding, diagnosis, and treatment of many diseases. Here, near-infrared (NIR) chemiluminescent (CL) carbon nanodots (CDs) are fabricated for the first time and their CL quantum yield can reach 9.98×10^{-3} einstein mol^{-1} , which is the highest value ever reported for CDs until now. Nanointegration of NIR CDs and peroxalate (P-CDs) through the bridging effect of amphiphilic triblock copolymer can serve as turn-on probes for the detection and imaging of hydrogen peroxide (H_2O_2). Considering high efficiency and large penetration depth of NIR photons, the P-CDs are employed in bioimaging H_2O_2 in vitro and in vivo, and the detection limit can reach 5×10^{-9} M, among the best reported of CDs-based sensors. Moreover, imaging of inflammatory H_2O_2 in a mouse model of peritonitis is achieved by employing the P-CDs as sensors. The results may provide a clue for the diagnosis and treatment of inflammation or cancers employing CL CDs as sensors.

1. Introduction

Reactive oxygen species (ROS), as significant reactive and signaling molecules in the process of intravital metabolism, play a great role in many biological processes.^[1–4] Among


the ROS molecules, hydrogen peroxide (H_2O_2) is prime reactive species, whose overproduction is closely related to various diseases, including inflammation, cancer, or neurological diseases.^[5–9] Thus it is of great importance in monitoring the concentration of H_2O_2 in living specimens. To this end, a number of mapping tools including “dark” biological processes and radiative recombination mechanism have been developed. Chemiluminescence (CL), a kind of light emission induced by energy transfer from chemical reactions, has evoked considerable interest as one ultrasensitive chemical analysis method with quantification and localization.^[10–12] Without auto-fluorescent interference and phototoxicity from high-energy excitation light, CL shows high signal-to-noise ratio and low perturbation in sensing H_2O_2 in vivo

compared to photoluminescence (PL) method.^[13–15] Moreover, unlike the bioluminescence probe requiring the activation of bioactive enzyme, CL imaging of H_2O_2 is a process of non-enzymatic reaction employing a H_2O_2 -responsive peroxalate that can transfer chemical energy to the CL emitter. Nevertheless, current CL reporters on H_2O_2 concentrate mainly on small-molecular dyes, semiconducting polymer, and aggregation induced emission nanoparticles, which suffer from low efficiency, short emission wavelength, and low chemical stability in highly oxidative ROS.^[16,17] Thereby, it is meaningful to develop new class of CL nanosensors for the imaging and detecting ROS in vitro and in vivo.

Carbon nanodots (CDs), which are considered as discrete quasi-spherical nanoparticles with sizes less than 10 nm, are one kind of promising nanomaterials in bioimaging, photocatalysis, optoelectronics, and sensing owing to its unique properties such as high emission efficiency, good biocompatibility, high photo-stability, and tunable luminescence.^[18–28] Recently, the CL properties of CDs in peroxalate– H_2O_2 system have been investigated, and it has been found that multicolor bright and persistent CL can be obtained from CDs.^[29] Therefore, it is practicable to develop versatile CL probes based on CDs to detect ROS via in vivo or in vitro imaging. In general, there are several advantages for CDs as the CL imaging probes: (i) CDs exhibit excellent light emission ability and the luminescence property can be tuned by different methods;^[30,31] (ii) CDs with emission

C.-L. Shen, Dr. Q. Lou, J.-H. Zang, Dr. K.-K. Liu, Prof. L. Dong, Prof. C.-X. Shan
Henan Key Laboratory of Diamond Optoelectronic Materials and Devices
Key Laboratory of Materials Physics
Ministry of Education
School of Physics and Microelectronics
Zhengzhou University
Zhengzhou 450052, China
E-mail: louqing1986@zzu.edu.cn; cxshan@zzu.edu.cn

Prof. S.-N. Qu
Joint Key Laboratory of the Ministry of Education
Institute of Applied Physics and Materials Engineering
University of Macau
Macau 999078, China

 The ORCID identification number(s) for the author(s) of this article can be found under <https://doi.org/10.1002/advs.201903525>.

© 2020 The Authors. Published by WILEY-VCH Verlag GmbH & Co. KGaA, Weinheim. This is an open access article under the terms of the Creative Commons Attribution License, which permits use, distribution and reproduction in any medium, provided the original work is properly cited.

DOI: 10.1002/advs.201903525

wavelength at near-infrared (NIR) region (beyond 650 nm) can be synthesized, which is particularly important for bioimaging due to the deep tissue penetration;^[32,33] (iii) the energy level of CDs can be modulated to reduce the energy interval with the energetic intermediate-1,2-dioxetanedione, which is beneficial to the electron transfer in the process of H₂O₂-activated luminescence and further enhances the CL quantum efficiency (QY) of CDs;^[14] (iv) the abundant surface radicals endow CDs with the good ability of drug carriers;^[34,35] (v) benign biocompatibility and high photostability of CDs make them promising application in CL bioimaging.^[36–42] Hence, it is significant to develop CD-based CL probes to generate luminescent signals in response to H₂O₂ and further provides a category of bioimaging for ROS.

Here, CDs with NIR CL have been synthesized with solvothermal method employing citric acid and urea as precursors in *N,N*-diethylformamide (DEF). The CDs exhibit an QY of 9.98×10^{-3} einstein mol⁻¹ in bis(2,4,5-trichloro-6-carboxyphenyl) oxalate (CPPO) and H₂O₂ solution, which is the highest value ever reported for the CL from CDs. In addition, P-CDs are transformed from NIR CDs and CPPO through the nanoscopic coaggregation process in the existence of amphiphilic polymeric conjugate (PEG-b-PPG-b-PEG). By virtue of the high efficiency and deep penetration of NIR emission, the P-CDs have been employed to bioimaging H₂O₂ in vitro and in vivo. Moreover, imaging of inflammatory H₂O₂ in a mouse model of peritonitis has been achieved by employing the P-CD as a sensor. The present work exhibits considerable potential for CDs as new class of CL probes for in vivo imaging applications in the diagnosis and treatment of inflammation or cancers.

2. Results and Discussion

In our previous report, it is found that multicolor PL and CL can be obtained from CDs by changing the degree of graphitization of the conjugated sp²-domains, implying that it is promising to excavate the application of CDs as novel probes for ROS sensing.^[29] However, a high CL QY and NIR emission of CD based probes are still urgent to be developed.

In this report, NIR CDs have been prepared with citric (1 g) and urea (2 g) in 10 mL DEF by one-step solvothermal strategy (160 °C for 8 h). DEF, as polar aprotic solvents, can exacerbate dehydration reaction and increase the conjugation degree of CDs due to effective dehydration reaction happened between citric acid and intramolecules with longer carbon chains (ethyl group from DEF).^[29,40–42] Transmission electron microscopy (TEM) has been used to characterize the morphology of the CDs, as shown in Figure 1a, where the CDs display a broad particle size distribution with an average diameter of around 4 nm. The high-resolution TEM (HRTEM) image and selected area electron diffraction (SAED) pattern reveal that the CDs have well-resolved lattice spacing of 0.34 nm, which corresponds to the (002) crystallographic plane of graphitic carbon. The X-ray diffraction (XRD) patterns of the CDs show a main peak at 23.1°, which can be attributed to the (002) planes of graphitic carbon (Figure S1, Supporting Information). The TEM and XRD results reflect the good crystalline structure of the CDs. Raman spectra also verify a high degree of crystallinity in the CDs owing to a large ratio of G band (1580 cm⁻¹) and D band (1350 cm⁻¹) of about 0.99 (Figure S2, Supporting Information). In addition, the deconvoluted high-resolution X-ray photoelectron spectra (XPS) for C1s, N1s, and O1s reveal that there are

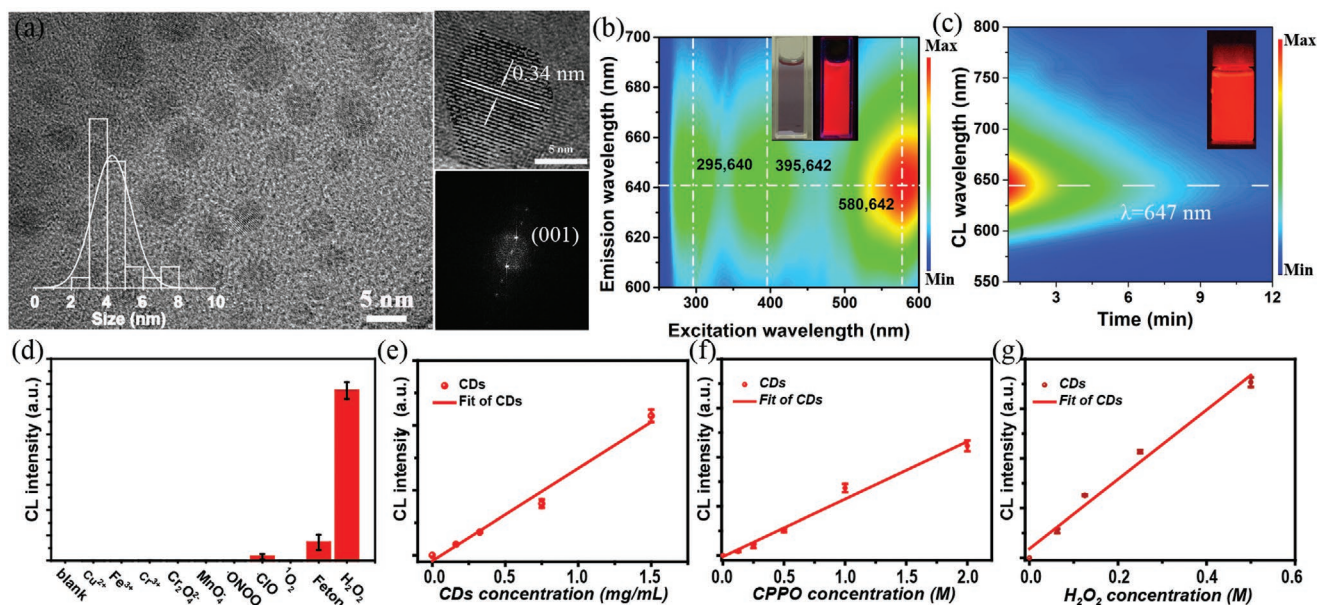


Figure 1. a) Transmission electron microscopy (TEM) images, high-resolution TEM (HRTEM) images, and selected area electron diffraction (SAED) pattern of the carbon nanodots (CDs) (inset: the size distribution of the CDs). b) 3D fluorescence mapping of the CDs in aqueous solution. (inset: the fluorescence image of the CDs under sunlight (left) and 365 nm UV excitation (right)). c) The decay spectra of the chemiluminescent (CL) from the CDs (inset: the photograph of the CL from the CDs). d) CL response of the CDs to various reactive oxygen species (ROS) in CL analysis instrument. CL signal intensities response of CDs to the concentration of e) CD, f) CPPO, and g) H₂O₂.

O- and N-containing functional groups on the surface of the CDs, which facilitates the surface modification for the CDs (Figures S3–S6, Supporting Information). The PL and CL properties of the CDs are illustrated in Figure 1b,c. Under the excitation of a 365 nm UV lamp, the aqueous solution of the CDs exhibits bright deep-red luminescence with the maximum PL emission peak at around 642 nm, extended to the NIR region (>650 nm). The excitation–emission 3D mapping pattern of the CDs shown in Figure 1b indicates that the emission center is almost immobile and ranged with three maximum excitation peaks at 295, 395, and 580 nm, which can be assigned to $\pi-\pi^*$ transition of sp^2 C, $n-\pi^*$ transition of conjugated C=O and Mie scattering due to the extended conjugation in the CD structure, respectively. The PL lifetime of 5.9 ns for the CDs can be calculated and obtained with a single exponential function (Figure S7, Supporting Information). Moreover, the CL emission spectra (≈ 647 nm) after adding CDs into CPPO and H_2O_2 solution present consistent spectra with the PL spectra, implying that the CD-based CL is originated from direct radiative recombination of the CDs under the chemical excitation (Figure 1c and Figures S8, S9, and Table S1, Supporting Information). The CL QY of the CDs is calculated to be 9.98×10^{-3} einstein mol^{-1} using lucigenin as the reference, which is the highest value ever reported even in CDs-based CL systems (Figures S10–S12 and Table S2, Supporting Information; Table 1). Meanwhile, the CL QY of the CDs in this work is much higher than the small-molecule dye, metal nanoparticles and is comparable to the semiconductor polymer nanoparticles (SPNs). The selectivity of the CL from CDs for the detection of H_2O_2 is further studied with CL analysis instrument. In

Table 1. Photoluminescence (PL) and chemiluminescent (CL) characteristics of the carbon nanodots (CDs).

Samples	λ_{em}^a [nm]	τ^b [ns]	λ_{em}^c [nm]	Φ_c^d [einstein mol^{-1}]
CDs	642	5.9	647	9.98×10^{-3}

^a) PL maximum peak; ^b) PL lifetime; ^c) CL maximum peak; ^d) CL quantum yield.

the presence of H_2O_2 , the CL signals of the CDs are far higher (>50 times) than that in the presence of other ROS, verifying that the CL system based on the CDs has a high selectivity to H_2O_2 (Figure 1d). Additionally, the CL intensity of the CDs is directly proportional to the concentration of the CDs, CPPO, and H_2O_2 , exhibiting the feasibility of quantification analysis of CL for probing H_2O_2 (Figure 1e–h and Figures S13–S16, Supporting Information). The efficient NIR CL and high selectivity promise the potential applications of the CDs as a CL probe to H_2O_2 .

For a better coaggregating CPPO (peroxalate esters) and hydrophilic CDs to form nanointegrated CDs (P-CDs), we have first developed one facile method to modulate CDs with lipophilic long chain (Figure S17, Supporting Information). As shown in Figure 2a, the water-soluble CDs can be modified by octadecylamine to synthesize oil-soluble NIR CDs (M-CDs) for using nanoscopic coaggregation. In the process, the M-CDs were formulated with CDs, octadecylamine, and mPEG-NH₂ in dimethylformamide (DMF) as illustrated in Experimental Section. With dichloromethane (CH_2Cl_2) as eluent, the hydrophobic M-CDs can be extracted from DMF with massive water and kept in dichloromethane (CH_2Cl_2) solution. As illustrated in the TEM images, the as-prepared M-CDs are

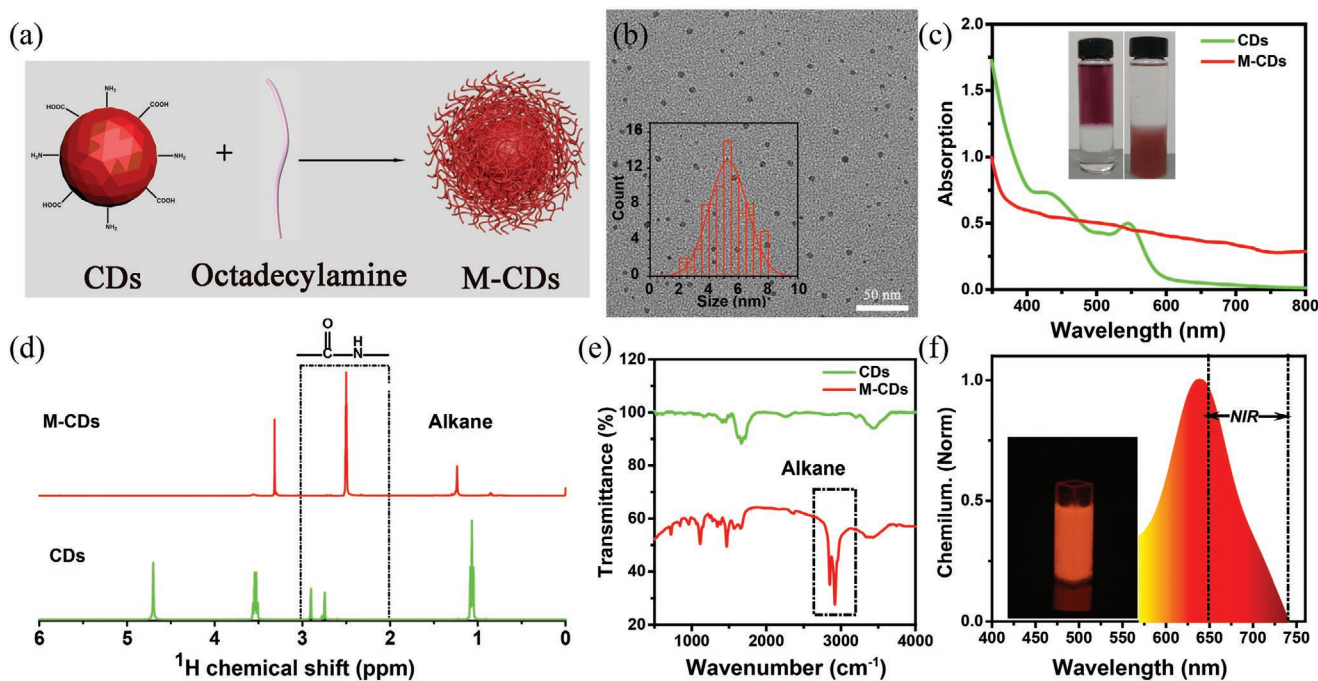


Figure 2. a) Schematic illustration of the preparation of the M-CDs. b) Transmission electron microscopy (TEM) images of the M-CDs (inset: the size distribution of the M-CDs). c) The UV–Vis absorption spectra of the CDs in aqueous and M-CDs in CH_2Cl_2 (inset: the distribution of CDs and M-CDs in $H_2O-CH_2Cl_2$). d) 1H NMR spectra of the CDs in D_2O and M-CDs in $CDCl_3$. e) Fourier transform infrared spectroscopy (FTIR) spectra of the CDs and M-CDs. f) Emission spectra after adding M-CDs solution into CPPO and H_2O_2 solution (inset: the image of the chemiluminescent (CL) M-CDs).

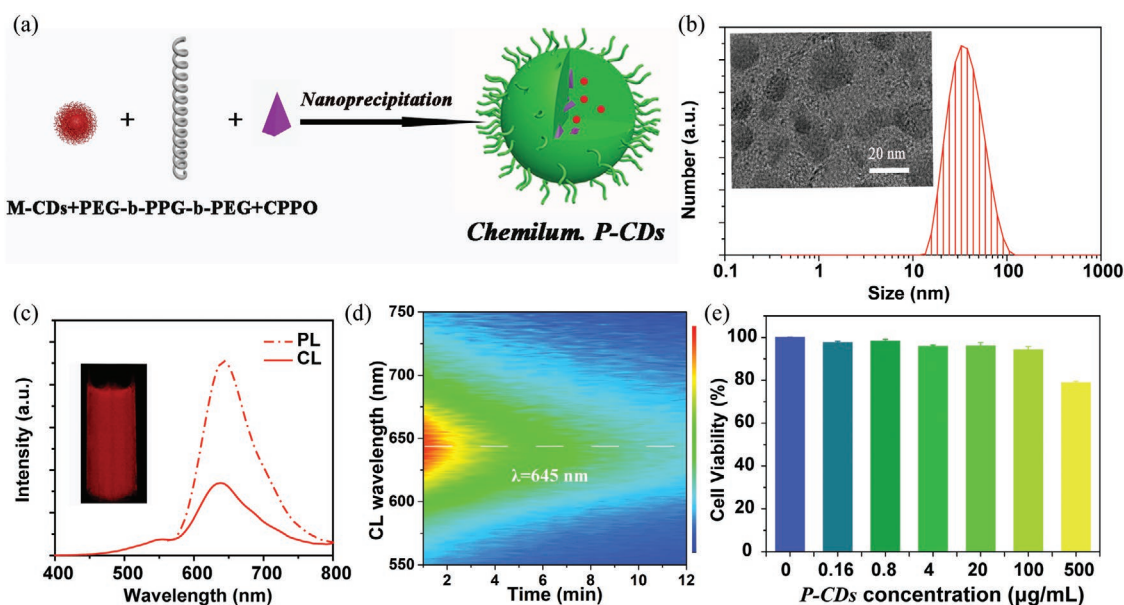


Figure 3. a) Schematic illustration of the preparation of the P-CDs. b) Dynamic light scattering (DLS) distribution of the P-CDs (inset: transmission electron microscopy (TEM) images of the P-CDs). c) The photoluminescence (PL) and CL emission spectra of the P-CDs, PL spectra is detected under 540 nm excitation for P-CDs aqueous solution and CL is detected by adding 1 mL, 10 mg mL⁻¹ P-CDs solution into 20 × 10⁻³ M H₂O₂ (inset: the photograph of P-CDs in H₂O₂ captured with 30 s). d) The dynamic CL spectra of the P-CDs. e) Cell viability of HeLa cells after 24 h incubation in the different concentration of the P-CDs.

spherical nanoparticles with an average diameter of around 5 nm, which is similar to the CDs shown in Figure 2b. As shown in Figure 2c, the UV-Vis absorption spectra of M-CDs are red-shifted compared to initial hydrophilic CDs. This bathochromic shift can be ascribed to the change of functional groups on the surface of the CDs. The inset of Figure 2c illustrates the good phase transfer from the water-soluble CDs to the oil-soluble CDs. ¹H nuclear magnetic resonance (NMR) and Fourier transform infrared spectroscopy (FTIR) have been employed to characterize the modification for the surface functional groups of the CDs and M-CDs (Figure 2d,e). The intense signals in the range of 2.2–2.9 ppm are corresponding to the protons of amine groups, verifying the substantial amide bond on the surface of M-CDs. The FTIR peaks at around 2900 cm⁻¹ can be ascribed to the stretching vibration of –CH₂–, which demonstrates the existence of octadecyl chains on the surface of the M-CDs. The above results indicate that hydrophobic of M-CDs results from the alkyl-chain functionalization. In addition, the excitation–emission matrix of the M-CDs in CH₂Cl₂ solution shows identical PL emission and excitation spectral profiles to the initial CDs solution (Figure 1b and Figure S18, Supporting Information). The CL spectra of the M-CDs also keep consistent with the original CDs, indicating that the modification has no obvious impact on the PL and CL emission properties of the CDs (Figure 2f and Figure S19, Supporting Information).

To explore the CDs as imaging probes for in vitro and in vivo applications, the aqueous dispersion of nanointegrated CDs and peroxalate particles (P-CDs) have been prepared through the nanoprecipitation of oil-soluble

M-CDs, CPPO, and amphiphilic PEG-b-PPG-b-PEG, as illustrated in Figure 3a and Experimental Section. By optimizing the loading weight of CDs in the P-CDs, the maximum CL QY of the P-CDs loaded with 2 mg M-CDs is calculated as about 1.87 × 10⁻³ einstein mol⁻¹, which is 7.6 times higher than those loaded with 2 mg water-soluble CDs (Table 2 and Figure S20, Supporting Information). Furthermore, the CL peak intensity of the P-CDs in water exhibits a 12.8 times enhancement when the surface of the CDs is modified from hydrophilic to hydrophobic, which may originate from the tight bridging between the oil-soluble M-CDs and the hydrophobic CPPO through the efficient hydrogen bond interaction. With the further increase in the loading weight of M-CDs, the P-CDs exhibit lower CL QYs, which may be generated from the aggregation induced quenching effect due to the strong interaction of high concentrations of M-CDs (Table 2 and Figures S21 and S22, Supporting Information). As determined by dynamic light scattering (DLS) in Figure 3b and Figures S23 and S24, Supporting Information, the obtained P-CDs have a number-weighted hydrodynamic diameter of about 40 nm, which is suitable for the usage in biomedical labeling and diagnostic applications. The TEM and HRTEM images present that P-CDs have polydispersed morphology with a wide size

Table 2. Chemiluminescent (CL) QYs of P-CDs with different M-CDs in 0.2 M H₂O₂.

Samples	Φ _C ^{a)} [einstein mol ⁻¹]	Φ _C ^{a)} [einsteins mol ⁻¹]	Φ _C ^{a)} [einsteins mol ⁻¹]	Φ _C ^{a)} [einsteins mol ⁻¹]	Φ _C ^{a)} [einsteins mol ⁻¹]
P-CDs	0.1 mg	1.0 mg	1.5 mg	2.0 mg	3.0 mg
	2.35 × 10 ⁻⁵	2.11 × 10 ⁻⁴	2.48 × 10 ⁻⁴	1.87 × 10 ⁻³	1.66 × 10 ⁻⁴

^{a)}CL quantum yield.

ranging from 20 to 100 nm, but the average diameter of P-CDs is about 40 nm (inset of Figure 3b and Figures S25–S27, Supporting Information). This is consistent with the results of DLS. And the well-resolved lattice spacing of 0.34 nm, attributed to the (002) crystallographic plane of M-CDs, can also be seen in the P-CDs. The luminescent property of the P-CDs in aqueous solution has been characterized by the excitation–emission matrices, illustrating a similar PL property as CDs solution (Figure 3c and Figure S28, Supporting Information). Moreover, the emission spectra after adding P-CDs into H₂O₂ solution have also been measured, as illustrated in Figure 3c, exhibiting a consistent CL emission with the corresponding steady-state PL spectra. The CL emission of the P-CDs can persist over tens of minutes (Figure 3d), which is long enough for the in vivo CL imaging experiments. In addition, the biocompatibility of P-CDs is also investigated, as shown in Figure 3e. More than 80% viability for HeLa cells can be obtained when the concentration of the P-CDs is 500 μg mL⁻¹, and indicating a low cytotoxicity, which is beneficial for the CL bioimaging applications.

With the merit of low toxicity, long persistent glowing, and deep penetration of NIR emission, the P-CDs can be employed as bioimaging probes to detect H₂O₂ in vitro and in vivo. Figure 4a illustrates the scheme of in vitro and in vivo CL imaging generated from P-CDs with the existence of

H₂O₂ from exogenous environment or endogenous disease. The practicability of P-CDs for in vitro imaging of exogenous H₂O₂ in aqueous has been first assessed by the PL and CL imaging with the IVIS imaging system. The PL and CL images are captured after adding P-CDs into different concentrations of H₂O₂ aqueous solution. As shown in Figure 4b and c, the PL intensity almost remain unchanged even when the addition of H₂O₂ is at a high concentration of 5 × 10⁻⁶ M, implying the PL imaging with P-CDs is not applicable to the detection of H₂O₂. In contrast, the CL intensity of the P-CDs presents a significant increase with increasing the H₂O₂ concentrations, as indicated in Figure 4c, where the CL intensity increases nearly linearly in the range of 0 to 100 × 10⁻⁹ M with a detection limit of 5 × 10⁻⁹ M (Figure S29, Supporting Information). The detection limit (5 × 10⁻⁹ M) is much smaller than the usual concentration of H₂O₂ (≈100 × 10⁻⁹ M) in living bodies, which is the best value ever reported for CDs based probes (Table S3, Supporting Information). To evaluate the ability of in vivo sensing the exogenous H₂O₂ for the P-CDs, the images of PL and CL intensity are also recorded when the anaesthetized nude mice are subcutaneously injected into the dorsal area with the P-CDs solution and different concentrations of H₂O₂. As shown in Figure 4d,e, the PL intensities almost keep constant with the increase of H₂O₂ concentration. Nevertheless, the CL intensity increases linearly with the increase of H₂O₂ concentration

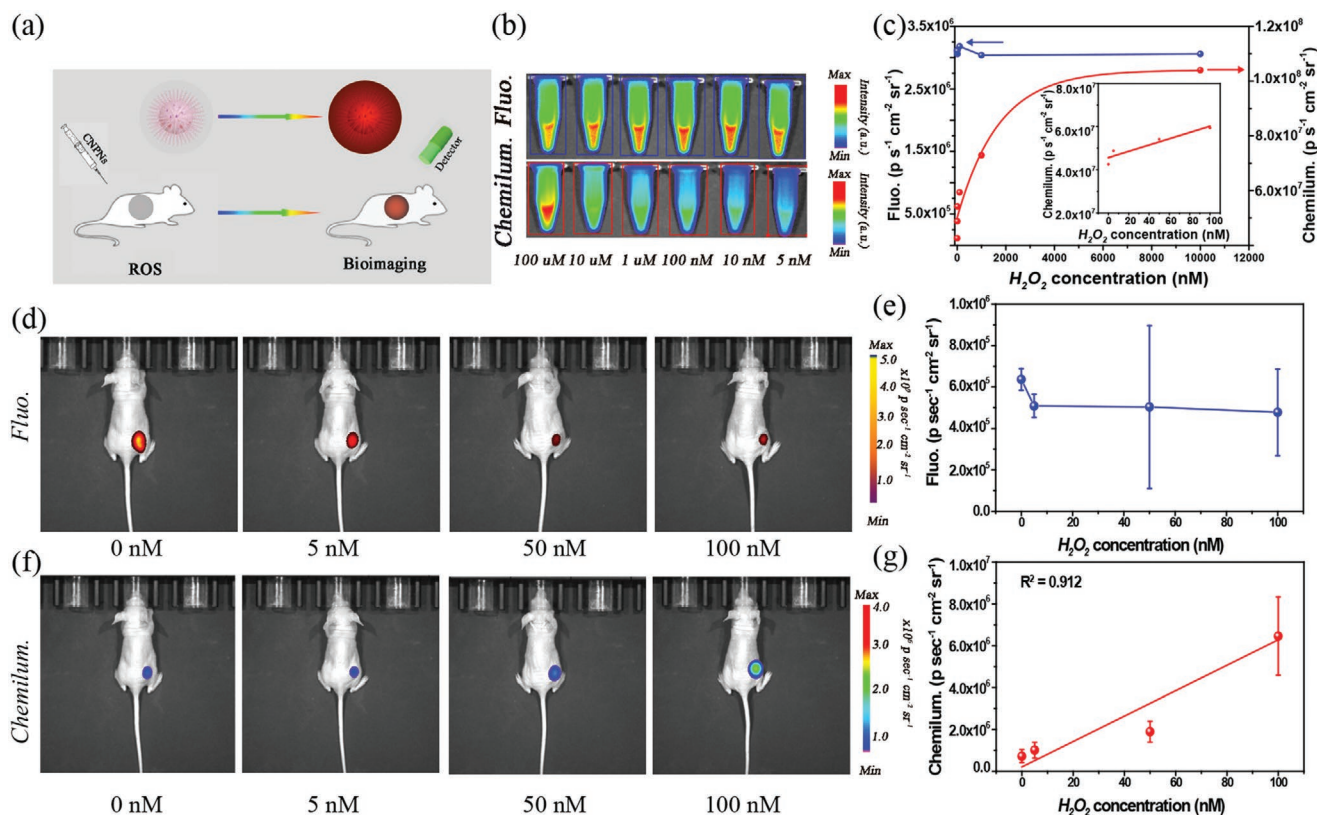


Figure 4. a) Schematic illustration of the exogenous sensing for reactive oxygen species (ROS). b) Photoluminescence (PL) and chemiluminescence (CL) images of P-CDs in the presence of different concentration of H₂O₂. c) PL and CL intensities of P-CDs under different concentration of H₂O₂. d) In vivo PL images of mice with the subcutaneous implantation of different concentration of H₂O₂. e) PL intensities as a function of the concentration of H₂O₂. f) In vivo CL images of mice with the subcutaneous implantation of different concentration of H₂O₂ (n = 3 mice per group). g) CL intensities as a function of the concentration of H₂O₂ (n = 3 mice per group).

from 0×10^{-9} to 100×10^{-9} M. Meanwhile, the CL intensity of the P-CDs with the existence of 5×10^{-9} M H_2O_2 is about 1.5-fold higher than that of the P-CDs alone.

Along with the high sensitivity, good biocompatibility, and potential deep tissue penetration, P-CDs are beneficial for detecting the endogenous H_2O_2 due to the abnormal variation in the body of living mice. Endogenous H_2O_2 is the significant metabolite when the body suffers from inflammation or cancers. Hence, the early diagnostics and treatment of these diseases can be achieved through monitoring the low concentration endogenous H_2O_2 . As a proof-of-concept, the inflammatory mouse models have been established through intraperitoneal injection of lipopolysaccharide (LPS), which can be used to induce the mouse model of peritonitis and further result in the generation of excessive H_2O_2 . The deep images of mouse models are captured for 3 min after the injection of P-CDs (0.3 mg mL^{-1} , 0.2 mL) at an early stage of peritonitis (4 h after LPS injection). As shown in Figure 5a,b, the PL intensities are almost unchanged for all the groups due to the structure resistance of P-CDs toward ROS. In contrast, the CL diagnostic signal for LPS-treated mice is 2.5-times higher than that for the control mice (Figure 5c,d). There is no CL when anesthetized mice were treated with intraperitoneal injection of M-CDs without nanointegration of peroxyate (left) or P-CDs without loading of M-CDs (right) after 4 h of LPS treatment, which can confirm that the presence of the isolated LPS cannot arise CL of CDs in vivo (Figure S30,

Supporting Information). After the inflamed mice by LPS are remedied with an antioxidant glutathione (GSH), CL signal intensity of the LPS + GSH treated mice shows a 40% reduction. The enhanced-to-reduced CL intensity can efficiently, as an inflamed-to-normal contrast signal, monitor the variation of inflammatory disease in living animals. The above results demonstrate that NIR CDs can act as a potential CL probe to diagnose and evaluate the state of an illness through sensitive in vivo bioimaging.

3. Conclusion

In summary, we have demonstrated efficient NIR emissive CDs-based CL system via energy transfer from the chemical reaction of peroxyate and H_2O_2 . With further modification, the CDs can be modified from hydrophilic to hydrophobic. P-CDs can be produced by combining the CDs, CPPO, and PEG-b-PPG-b-PEG through the nanoscopic coaggregation. The NIR P-CDs generate good in vitro and in vivo CL signals in response to H_2O_2 with a linear range from 0 to 100×10^{-9} M and a low detection limit of 5×10^{-9} M. Furthermore, the P-CDs are proved to be a potential CL probe for bioimaging H_2O_2 in the inflammation-related diseases in living mice. The results reported in this paper may provide a clue for the diagnosis and treatment of inflammation or cancers employing CL CDs as sensors.

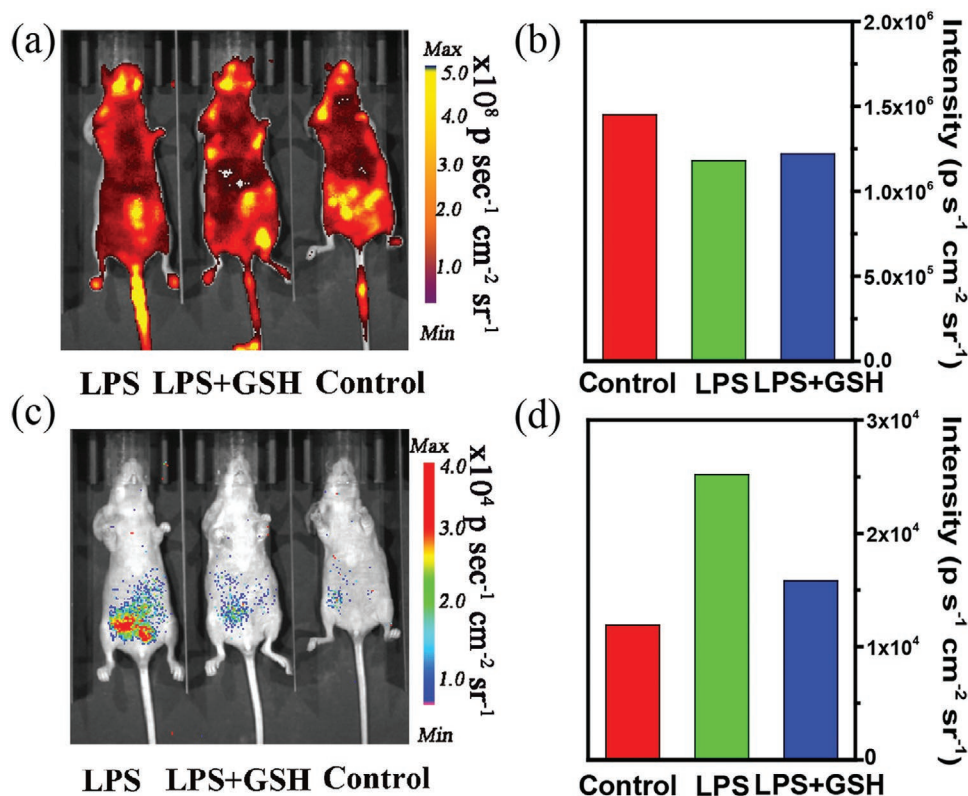


Figure 5. In vivo imaging of endogenous H_2O_2 in the mouse model of peritonitis. a) Photoluminescence (PL) and c) chemiluminescent (CL) images of mice intraperitoneally treated with lipopolysaccharide (LPS), LPS plus glutathione (GSH) and saline, followed by an intraperitoneal injection of P-CDs at $t = 4$ h later. Quantification of b) PL and d) CL intensities for the in vivo images.

4. Experimental Section

Synthesis and Purification of CDs: An amount of 1 g citric acid and 2 g urea were dispersed in 10 mL of DEF. The mixtures were added into Teflon-lined stainless autoclave (20 mL). Then the sealed autoclave vessels were placed into an electric oven, which was set at 160 °C and hold for 8 h. The resulting solvents were purified via silica column chromatography using DMF as the eluent, and then the as-prepared CDs were precipitated with absolute ethyl alcohol and collected by vacuum drying at 60 °C for 1 day. The final products were collected for characterizations and further used.

Synthesis and Purification of M-CDs: An amount of 0.2 g CDs powder, 0.8 g octadecylamine, and 0.1 g mPEG-NH₂ were dispersed into 50 mL DMF, where the octadecylamine was used to switch the water–oil soluble of the CDs and mPEG-NH₂ was used to increase the cross-linking of CDs and octadecylamine. After stirring with air flow for 12 h under 60 °C, 10 mL mixture was dispersed in 20 mL CH₂Cl₂. With dichloromethane CH₂Cl₂ as eluent, the hydrophobic M-CDs can be extracted from DMF with massive water and kept in CH₂Cl₂ solution. The as-prepared M-CDs were collected by vacuum drying at 60 °C for 1 day. The final products were collected for characterizations and further used.

Synthesis of P-CDs: PEG-b-PPG-b-PEG (40 mg), CPPO (4 mg), and different mass of M-CDs (0.1, 1.0, 1.5, 2, and 3 mg) were dispersed into CH₂Cl₂ (5.0 mL) solution. After CH₂Cl₂ was evaporated with air flow, the powder was redispersed into 2 mL deionized water and filtered through a 0.22 μm PVDF syringe driven filter (Millipore). The formed P-CDs suspension was finally concentrated to different concentrations by ultrafiltration and used immediately for experiments.

CL QYs of CDs and P-CDs: The CL QYs of the CDs and P-CDs were measured using lucigenin with H₂O₂ as oxidant with a known QY of 8.3 × 10⁻³ einstein mol⁻¹ at pH 11 according to the previous literatures.^[29] According to the CL spectra and kinetic curves, the CL QYs were calculated according to the following equations:

$$\phi_{CL} = \frac{Q \times f_{luc} \times f_{photo}}{n} \text{ (einstein mol}^{-1}\text{)} \quad (1)$$

$$f_{luc} = \frac{\phi_{luc} \times n_{luc}}{Q_{luc}} \quad (2)$$

$$f_{photo} = \frac{f(\lambda_s)}{f(\lambda_{luc})} \quad (3)$$

Where ϕ_{CL} is the CL QYs of CDs and P-CDs, Q is the total light emission obtained by integration of emission intensity under time curves. f_{luc} is obtained by measuring the emission kinetics of lucigenin reaction performed in standard conditions. f_{photo} is obtained from the sensitivity at the emission wavelength ($\lambda_{max} = 475$ nm) of the lucigenin standard, $f(\lambda_{luc})$, and the emission of the CDs and P-CDs, $f(\lambda_s)$. n is the number of moles of lucigenin (n_{luc}) or the number of moles of CPPO.

In Vitro Characterization of P-CDs: For the quantitative analysis, P-CDs (10 mg mL⁻¹, 1 mL) were placed in EP tubes. After addition of different concentrations (0 × 10⁻⁹, 5 × 10⁻⁹, 50 × 10⁻⁹, 100 × 10⁻⁹, 1 × 10⁻⁶, and 5 × 10⁻⁶ M) of H₂O₂, both PL and CL imaging were performed using an IVIS spectrum imaging system. CL images were acquired for 30 s with open filter or emission at 640 ± 10 nm, and fluorescence images were acquired for 0.1 s with excitation of 550 ± 10 nm, and emission at 640 ± 10 nm. The media pH 7.4 was controlled using phosphate buffer saline (PBS) buffer solution.

Cytotoxic Evaluation: The PBS solution with different concentrations (0, 0.16, 0.8, 4, 20, 100, and 500 μg mL⁻¹) of P-CDs was used for incubating the Hela cells for 24 h at 37 °C. Then, the cell viability of Hela cell was tested using standard MTT method for assessing the cytotoxicity of the P-CDs.

In Vivo CL Imaging: All animal studies were performed in compliance with the Guide Care and Use of Laboratory Animals proposed by the National Institutes of Health. All procedures and protocols were

approved by the Animal Ethics Committee at Zhengzhou University (Zhengzhou, China). For in vivo bioimaging exogenous H₂O₂, P-CDs (10 mg mL⁻¹) were mixed with different concentrations (0 × 10⁻⁹, 5 × 10⁻⁹, 50 × 10⁻⁹, and 100 × 10⁻⁹ M) of H₂O₂, and the P-CD suspension (0.1 mL) was injected subcutaneous into the dorsal of anaesthetized mice (2% isoflurane in oxygen). The media pH 7.4 was controlled using PBS buffer solution. CL images were obtained with a 3 min acquisition time with open filter or emission at 640 ± 10 nm, and fluorescence images were acquired for 30 s with excitation of 550 ± 10 nm, and emission at 640 ± 10 nm.

To image endogenous H₂O₂ in the mouse model of peritonitis, mice (6–8 weeks old) were injected intraperitoneally with LPS (8 mg kg⁻¹). For the inhibitor study, mice were treated intraperitoneally 5 min before LPS treatment using 200 mg kg⁻¹ GSH. The control mice were treated only using 200 mg kg⁻¹ saline. After 4 h, anesthetized mice (2% isoflurane in oxygen) were treated with intraperitoneal injection of P-CDs (10 mg mL⁻¹, 0.2 mL). CL images were captured with a 3 min acquisition time with open filter using the IVIS spectrum imaging system. Fluorescence images were captured with a 0.1 s acquisition time with excitation of 550 ± 10 nm, and emission at 640 ± 10 nm using the IVIS spectrum imaging system.

More details about the characterization of material and data are demonstrated in Supporting Information.

Supporting Information

Supporting Information is available from the Wiley Online Library or from the author.

Acknowledgements

The authors gratefully acknowledge the support for this research from the National Natural Science Foundation of China (51602288, 11904326, and U1604263), and the Natural Science Foundation of Henan Province (182300410281).

Conflict of Interest

The authors declare no conflict of interest.

Keywords

bioimaging, carbon nanodots, chemiluminescence, reactive oxygen species, sensors, turn-on probes

Received: December 8, 2019

Revised: February 7, 2020

Published online: March 9, 2020

- [1] B. D'Autr aux, M. B. Toledano, *Nat. Rev. Mol. Cell Biol.* **2007**, *8*, 813.
- [2] M. Wang, *Nat. Rev. Nephrol.* **2019**, *15*, 61.
- [3] N. Gong, X. Ma, X. Ye, Q. Zhou, X. Chen, X. Tan, S. Yao, S. Huo, T. Zhang, S. Chen, X. Teng, X. Hu, J. Yu, Y. Gan, H. Jiang, J. Li, X. Liang, *Nat. Nanotechnol.* **2019**, *14*, 379.
- [4]  . Canli, A. M. Nicolas, J. Gupta, F. Finkelmeier, O. Goncharova, M. Pesic, T. Neumann, D. Horst, M. L ower, U. Sahin, F. R. Greten, *Cancer Cell* **2017**, *32*, 869.
- [5] A. J. Shuhendler, K. Pu, L. Cui, J. P. Uetrecht, J. Rao, *Nat. Biotechnol.* **2014**, *32*, 373.

- [6] W. Dröge, *Physiol. Rev.* **2002**, *82*, 47.
- [7] H. Blaser, C. Dostert, T. W. Mak, D. Brenner, *Trends Cell Biol.* **2016**, *26*, 249.
- [8] C. Tapeinos, A. Pandit, *Adv. Mater.* **2016**, *28*, 5553.
- [9] S. Bhattacharya, R. Sarkar, S. Nandi, A. Porgador, R. Jelinek, *Anal. Chem.* **2017**, *89*, 830.
- [10] Y. Chen, A. J. H. Spiering, S. Karthikeyan, G. W. M. Peters, E. W. Meijer, R. P. Sijbesma, *Nat. Chem.* **2012**, *4*, 559.
- [11] Y. Liu, W. Shen, Q. Li, J. Shu, L. Gao, M. Ma, W. Wang, H. Cui, *Nat. Commun.* **2017**, *8*, 1003.
- [12] S. Kwak, J. P. Giraldo, M. H. Wong, V. B. Koman, T. T. S. Lew, J. Ell, M. C. Weidman, R. M. Sinclair, M. P. Landry, W. A. Tisdale, M. S. Strano, *Nano Lett.* **2017**, *17*, 7951.
- [13] Y. Lee, C. Lim, A. Singh, J. Koh, J. Kim, I. C. Kwon, S. Kim, *ACS Nano* **2012**, *6*, 6759.
- [14] X. Zhen, C. Zhang, C. Xie, Q. Miao, K. L. Lim, K. Pu, *ACS Nano* **2016**, *10*, 6400.
- [15] Q. Miao, K. Pu, *Adv. Mater.* **2018**, *30*, 1801778.
- [16] F. Hu, S. Xu, B. Liu, *Adv. Mater.* **2018**, *30*, 1801350.
- [17] O. Green, S. Gnaim, R. Blau, A. Eldar-Boock, R. Satchi-Fainaro, D. Shabat, *J. Am. Chem. Soc.* **2017**, *139*, 13243.
- [18] C. Zhu, Y. Fu, C. Liu, Y. Liu, L. Hu, J. Liu, I. Bello, H. Li, N. Liu, S. Guo, H. Huang, Y. Lifshitz, S. Lee, Z. Kang, *Adv. Mater.* **2017**, *29*, 1701399.
- [19] Z. Wang, F. Yuan, X. Li, Y. Li, H. Zhong, L. Fan, S. Yang, *Adv. Mater.* **2017**, *29*, 1702910.
- [20] X. Miao, D. Qu, D. Yang, B. Nie, Y. Zhao, H. Fan, Z. Sun, *Adv. Mater.* **2018**, *30*, 1704740.
- [21] F. Yuan, Z. Wang, X. Li, Y. Li, Z. Tan, L. Fan, S. Yang, *Adv. Mater.* **2017**, *29*, 1604436.
- [22] S. Bhattacharya, R. S. Phatake, S. Nabha Barnea, N. Zerby, J. Zhu, R. Shikler, N. G. Lemcoff, R. Jelinek, *ACS Nano* **2019**, *13*, 7396.
- [23] S. Qu, X. Liu, X. Guo, M. Chu, L. Zhang, D. Shen, *Adv. Funct. Mater.* **2014**, *24*, 2689.
- [24] F. Wang, Z. Xie, H. Zhang, C. Liu, Y. Zhang, *Adv. Funct. Mater.* **2011**, *21*, 1027.
- [25] S. N. Baker, G. A. Baker, *Angew. Chem., Int. Ed.* **2010**, *49*, 6726.
- [26] K. K. Liu, S. Y. Song, L. Z. Sui, S. X. Wu, P. T. Jing, R. Q. Wang, Q. Y. Li, G. R. Wu, Z. Z. Zhang, K. J. Yuan, C. X. Shan, *Adv. Sci.* **2019**, *6*, 1900766.
- [27] S. Bhattacharya, R. Sarkar, B. Chakraborty, A. Porgador, R. Jelinek, *ACS Sens.* **2017**, *2*, 1215.
- [28] N. Shauloff, S. Bhattacharya, R. Jelinek, *Carbon* **2019**, *152*, 363.
- [29] C. L. Shen, Q. Lou, C. F. Lv, J. H. Zang, S. N. Qu, L. Dong, C. X. Shan, *Adv. Sci.* **2019**, *6*, 1802331.
- [30] S. Hu, A. Trinchì, P. Atkin, I. Cole, *Angew. Chem., Int. Ed.* **2015**, *54*, 2970.
- [31] S. Zhu, Q. Meng, L. Wang, J. Zhang, Y. Song, H. Jin, K. Zhang, H. Sun, H. Wang, B. Yang, *Angew. Chem., Int. Ed.* **2013**, *52*, 3953.
- [32] S. Lu, L. Sui, J. Liu, S. Zhu, A. Chen, M. Jin, B. Yang, *Adv. Mater.* **2017**, *29*, 1603443.
- [33] K. Holá, M. Sudolská, S. Kalytchuk, D. Nachtigallová, A. L. Rogach, M. Otyepka, R. Zbořil, *ACS Nano* **2017**, *11*, 12402.
- [34] H. Yu, Y. Xue, Y. Li, *Adv. Mater.* **2019**, *31*, 1803101.
- [35] J. Tang, B. Kong, H. Wu, M. Xu, Y. Wang, Y. Wang, D. Zhao, G. Zheng, *Adv. Mater.* **2013**, *25*, 6569.
- [36] A. Zhu, Q. Qu, X. Shao, B. Kong, Y. Tian, *Angew. Chem., Int. Ed.* **2012**, *51*, 7185.
- [37] S. Lu, G. Xiao, L. Sui, T. Feng, X. Yong, S. Zhu, B. Li, Z. Liu, B. Zou, M. Jin, J. S. Tse, H. Yan, B. Yang, *Angew. Chem., Int. Ed.* **2017**, *56*, 6187.
- [38] W. Li, Z. Zhang, B. Kong, S. Feng, J. Wang, L. Wang, J. Yang, F. Zhang, P. Wu, D. Zhao, *Angew. Chem., Int. Ed.* **2013**, *52*, 8151.
- [39] J. Liu, N. Wang, Y. Yu, Y. Yan, H. Zhang, J. Li, J. Yu, *Sci. Adv.* **2017**, *3*, e1603171.
- [40] D. Qu, M. Zheng, J. Li, Z. Xie, Z. Sun, *Light: Sci. Appl.* **2015**, *4*, e364.
- [41] R. Sekiya, Y. Uemura, H. Murakami, T. Haino, *Angew. Chem., Int. Ed.* **2014**, *53*, 5619.
- [42] Z. Tian, X. Zhang, D. Li, D. Zhou, P. Jing, D. Shen, S. Qu, R. Zboril, A. L. Rogach, *Adv. Opt. Mater.* **2017**, *5*, 1700416.